Serine 85 in Transmembrane Helix 2 of Short-Wavelength Visual Pigments Interacts with the Retinylidene Schiff Base Counterion†

Abhiram Dukkipati,‡,§ Bryan W. Vought,‡,|| Deepak Singh,‡,⊥ Robert R. Birge,*,‡,# and Barry E. Knox*,§

Departments of Biochemistry and Molecular Biology and of Ophthalmology, SUNY Upstate Medical University, 750 East Adams Street, Syracuse, New York 13210, and Departments of Chemistry and Biology, Syracuse University, 111 College Place, Syracuse, New York 13244-4100

Received June 27, 2001; Revised Manuscript Received October 10, 2001

ABSTRACT: Short-wavelength cone visual pigments (SWS1) are responsible for detecting light from 350 to 430 nm. Models of this class of pigment suggest that TM2 has extensive contacts with the retinal binding pocket and stabilizes interhelical interactions. The role of TM2 in the structure−function of the *Xenopus* SWS1 (VCOP, $\lambda_{max} = 427$ nm) pigment was studied by replacement of the helix with that of bovine rhodopsin and also by mutagenesis of highly conserved residues. The TM2 chimera and G78D, F79L, M81E, P88T, V89S, and F90V mutants did not produce any significant spectral shift of the dark state or their primary photointermediate formed upon illumination at cryogenic temperatures. The mutant G77R (responsible for human tritanopia) was completely defective in folding, while C82A and F87T bound retinal at reduced levels. The position S85 was crucial for obtaining the appropriate spectroscopic properties of VCOP. S85A and S85T did not bind retinal. S85D bound retinal and had a wild-type dark state at room temperature and a red-shifted dark state at 45 K and formed an altered primary photointermediate. S85C absorbed maximally at 390 nm at neutral pH and at 365 nm at pH >7.5. The S85C dark state was red shifted by 20 nm at 45 K and formed an altered primary photointermediate. These data suggest that S85 is involved in a hydrogen bond with the protonated retinylidene Schiff base counterion in both the dark state and the primary photointermediate.

Vertebrate vision is mediated by five distinct families of visual pigments (*1*). These pigments are prototypical heptahelical GPCRs,[1] with an 11-*cis*-retinal chromophore covalently bound via a Schiff base to a lysine in transmembrane helix 7 of the opsin apoprotein (*2*, *3*). Absorption of a photon isomerizes 11-*cis*-retinal to *all*-*trans*-retinal, resulting in a series of conformational changes in the protein (*4*, *5*). The final active conformation, meta II, activates the G protein, transducin, initiating the downstream signaling cascade (*6*). Unlike other GPCRs, in which the ligand acts as an agonist, the covalently bound retinal acts as an antagonist and prevents the receptor from activating the signaling cascade in the dark.

There are two fundamentally different realms of photoreceptor function: dim light (scotopic) typically taking place in rods and photopic illuminance taking place in cones (*7*). In response to the wide-ranging lighting conditions in which cones and rods function, markedly different response characteristics have developed (*8*). Cone responses adapt rapidly to changes in light intensity and are noisy but do not saturate to ambient light levels. Additionally, cones have adapted to respond to a wide spectral range of light, from the ultraviolet to far-red. Cone visual pigments are responsible for spectral sensitivities of cones and may play an important role in determining the response dynamics of the cell. Cone visual pigments have a number of properties that distinguish them from the rhodopsins: a shorter lifetime of the active protein conformation compared to rhodopsins and rapid recovery postbleaching. Moreover, the retinal binding pocket is more solvent accessible in the dark, demonstrated by hydroxylamine-induced bleaching. The molecular features that determine the differences between rod and cone pigment properties have not been well characterized. Numerous mutations that alter the spectral tuning and several that change the photobleaching pathway in a variety of rod and cone opsins have not yet clarified these properties (*1*, *9*−*14*).

The recent elucidation of the structure of bovine rhodopsin to 2.8 Å (*15*) opens the way for crucial insights into the

† This work was supported in part by NIH Grants GM-34548 (to R.R.B.) and EY-12975 and EY-11256 (to B.E.K.), the W. M. Keck Center for Molecular Electronics at Syracuse University, and a grant from the Research to Prevent Blindness Foundation.

* Correspondence should be addressed to either B.E.K. [tel, (315) 464-8719; fax, (315) 464-8750; e-mail, knoxb@mail.upstate.edu] or R.R.B. [tel, (860) 486-6720; fax, (860) 486-2981; e-mail, rbirge@uconn.edu].

‡ Syracuse University.

§ SUNY Upstate Medical University.

|| Present address: Department of Biological Chemistry and Molecular Pharmacology, Harvard Medical School, 240 Longwood Ave., Boston, MA 02115.

⊥ Present address: GeneFormatics Inc., 5830 Oberlin Drive, Suite 200, San Diego, CA 92121.

Present address: Departments of Chemistry and Molecular and Cell Biology, University of Connecticut, 55 North Eagleville Road, Storrs, CT 06269.

[1] Abbreviations: GPCR, G protein coupled receptor; VCOP, violet cone opsin; TM no., transmembrane helix no.; SWS, short-wavelength sensitive; RH, rhodopsins; M/LWS, medium/long wavelength sensitive; nm, nanometers; PSS(*xyz*), photostationary state generated by illumination at wavelength *xyz* in nanometers; B1, photostationary state 395 formed at 45 K; B2, photostationary state 395 formed at 75 K; DM, *N*-dodecyl *β*-D-maltoside; ROS, rod outer segment; batho and lumi, discrete thermal intermediates of the visual opsin bleaching pathway.

10.1021/bi011354l CCC: $20.00
Published on Web 11/21/2001

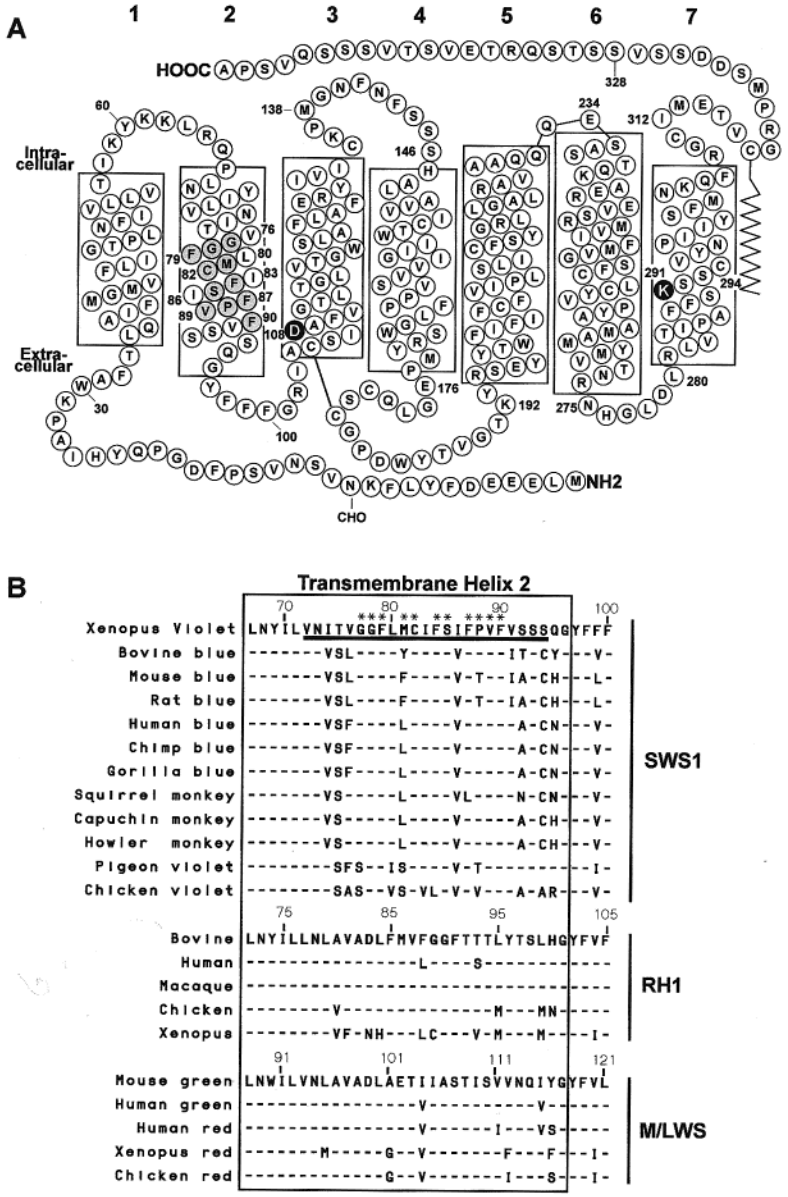

FIGURE 1: (A) Secondary structure model of the violet cone opsin (VCOP). The counterion (D108) and the site of retinal attachment (K291) are indicated. Residues in transmembrane helix 2 (TM2) that were mutated are highlighted in gray. (B) Sequence alignment of TM2 residues of selected opsins from SWS1, RH1, and M/LWS opsins (also indicated by the boxed sequences). The residues that were point mutated in VCOP TM2 are indicated with an asterisk. The region of helix 2 in VCOP that was replaced with the corresponding region of bovine rhodopsin is underlined.

structural basis for cone opsin function. An important feature of the rhodopsin structure is the central position of TM2 in the interhelical bundle and the retinylidene Schiff base environment. The cytoplasmic ends of TM2 and TM4 are in close proximity and diverge within the membrane, permitting the penetration of TM3 at the extracellular end. Presumably, such a conformation is necessary for the optimal orientation between the Schiff base counterion (E113) and the protonated retinylidene Schiff base at K296. In addition, there is a large kink in the center of TM2 (created by two glycines), in close proximity to the Schiff base counterion. In fact, acidic mutations at G90 can compete for the native counterion−Schiff base interaction (*16*, *17*). A number of other residues in TM2 are also located in the vicinity of the Schiff base or are important for contributing to interhelical interactions.

To understand how TM2 contributes to cone pigment function, we initiated a detailed mutagenesis and spectroscopic study of conserved residues from TM2 in a short-wavelength cone visual pigment from *Xenopus* (VCOP, Figure 1A) which absorbs at 427 nm (*18*). This cone pigment is attractive for study because it is efficiently expressed in COS1 cells and stable in the dark in a detergent-solubilized delipidated form. We have elucidated the complete photobleaching pathway of this pigment and determined that the Schiff base is protonated in the dark state (*19*). Moreover, we have shown that this pigment is able to activate transducin and has a short-lived active meta II conformation, and the apoprotein is able to regenerate much more efficiently with 11-*cis*-retinal compared to rhodopsin (*20*). Thus, it exhibits in vitro many of the properties expected for cone pigments. Finally, we have recently identified the retinylidene Schiff base counterion and investigated the role of this residue in regulating the photobleaching cascade (Babu et al., in press). Here, we show that serine 85 in TM2 is absolutely crucial for retinal binding of VCOP and that this residue interacts

with the retinylidene Schiff base counterion in both the dark and the primary photointermediate trapped at cryogenic temperatures.

MATERIALS AND METHODS

Preparation and Expression of VCOP Mutants. All single amino acid replacements were made in the *Eco*RI−*Sal*I VCOP fragment subcloned into a modified pBlueScript (Stratagene) plasmid using the QuikChange kit (Stratagene). The bovine rhodopsin TM2−VCOP chimera cDNA was prepared by restriction fragment replacement, in which the *Hin*dIII−*Bsa*HI fragment of VCOP (encoding amino acids 62−108) was replaced with a synthetic oligonucleotide corresponding to amino acids 62−71 from VCOP, 72−94 with the bovine rhodopsin amino acids 77−99, and 95−108 with the corresponding VCOP amino acids. All mutant plasmid cDNAs were sequenced on both strands and then cloned into the pMT5 expression vector. The resulting plasmid had the cDNA containing the codons coding for the first of 328 amino acids of the mutant opsin fused in frame with the codons coding for the last 14 amino acids of bovine rhodopsin which serves as an epitope tag (*21*). The mutants were expressed in COS1 cells by transient transfection, purified by immunoaffinity chromatography, and analyzed by Western blots as previously described (*18*, *22*).

UV−Vis Spectroscopy. Conventional UV−vis spectroscopy was done using a Beckman DU-640 spectrophotometer with a 1 cm path length. For light − dark difference spectra, four spectra were obtained in the dark, the samples were bleached in white light with a projector lamp (300 W, EXR-5, Wiko, Inc.) from a distance of 30 cm for 1 min, and four spectra were recorded. The total radiant energy of the white light measured by an optometer (Graseby Optronics) was 8 mW. For acid−base titration of the S85C mutant, the concentrated protein was transferred to a buffer containing 10 mM potassium phosphate (pH 6.6) and 0.1% DM by extensive washing with this buffer in a Centricon C-30 filter (Amicon). This avoided the precipitation of magnesium at elevated pH. We have found that VCOP is stable in phosphate buffer for at least 4 weeks. The pH of the sample was lowered or raised incrementally using calculated volumes of 0.1 M phosphoric acid or 0.1 M NaOH, respectively. Subtraction of light scattering using a $1/\lambda^4$ correction factor was done for all room temperature mutant spectra (except VCOP and S85C) using the FITSPECTRA program (R. R. Birge, unpublished and available upon request). Light − dark difference spectra were calculated by averaging four spectra in SigmaPlot (Jandel Scientific).

Low-Temperature Spectroscopy. This was done as reported previously (*19*, *22*). Purified samples were made up to 67% glycerol and 0.05% DM. The samples were thermally equilibrated at 45 K for 1 h and illuminated with 395 nm light to generate a maximum amount of the bathochromic photostationary state (PSS395). A photostationary state (PSS) is generated when further illumination does not produce any spectral shifts. The sample was illuminated with 500 nm light to generate the reverse photostationary state (PSS500). The sample was gradually warmed to 75 K and allowed to thermally equilibrate for 1 h. Then 395 nm illumination was used to generate a maximum amount of PSS395, and 500 nm illumination was then used to generate PSS500. From here on, PSS395 formed at 45 K will be referred to as B1 while PSS395 formed at 75 K will be referred to as B2. All photoconversions were done using a 100 W HgXe arc lamp through a monochromator. Coupling optics maximized illumination of the sample while in the cold tip.

Derivation of the Batho Spectra of S85C and S85D. We did not have sufficient amounts of the S85C and S85D pigments to permit HPLC analysis of photostationary state composition. Thus, rigorous assignment of the batho spectra for S85C and S85D was not possible. However, we noted that it was possible to assign the relative spectrum of the batho state by assuming that the photostationary state contains only two components, the all-trans (batho) species and the 11-cis (dark) species. The batho spectrum, $B(\xi)$, is then given by the formula:

$$B(\xi) = b_\lambda^{-1}\mathrm{PSS}_\lambda(\xi) + \frac{b_\lambda - 1}{b_\lambda}A(\xi)$$

where ξ is the energy (or wavelength) coordinate of the spectra, $\mathrm{PSS}_\lambda(\xi)$ is the photostationary state spectrum created via excitation at wavelength λ, b_λ is the fractional amount of the batho state in $\mathrm{PSS}_\lambda(\xi)$, and $A(\xi)$ is the spectrum of the initial, dark state (11-cis chromophore). Because both $A(\xi)$ and $\mathrm{PSS}_\lambda(\xi)$ are the measured spectra, the only unknown in this equation is the scalar constant, b_λ. Upper and lower limits for this constant are easily determined by visually monitoring the calculated batho spectrum, $B(\xi)$, while varying b_λ within the possible limits of 0 (no conversion) to 1 (full conversion). One can find a reasonable estimate for b_λ by assuming that the batho spectrum has no spectral features identical to the λ_{max} band of the dark spectrum. There are no known batho spectra which violate this assumption. One can then monitor the calculated batho spectrum and reject all spectra which contain a spectral feature identical to the dark λ_{max} band (b_λ is too small). We will call this lower limit of b_λ, b_λ^{min}. We can set the upper limit to b_λ by monitoring for negative spectral features (physically impossible) or negative going bands that correlate with the λ_{max} band of the dark spectrum. We will call the upper limit of b_λ obtained in this approach, b_λ^{max}. By choosing a value for b_λ that is the average of the above two limits, a realistic (but not rigorously accurate) batho spectrum is produced. In the present case, this approach generates batho spectra that are reliable in terms of absorption maximum but which have large uncertainty in full width at half-maximum and relative absorptivity. The problem derives not only from the uncertainty in assigning b_λ but also in the formation of small amounts of the isopigment (9-cis chromophore) in the photostationary state. While the presence of the 9-cis species does not have a significant impact on the calculated batho absorption maximum, uncertainty in the composition was an additional hindrance in assigning the extinction coefficient. For the above reasons, we report here only the normalized batho spectra in Figure 8. We estimate the absorption maxima to be accurate to ±4 nm.

Modeling of the VCOP Retinal Binding Site. The binding site model shown in Figure 10 was generated by using the VCOP binding site model from ref *19*, which was based on a similarity replacement of the rhodopsin side chains with the corresponding residues of violet cone opsin. The protein backbone was harmonically constrained, and the residue side

Table 1: Spectral Properties of VCOP Mutants

mutant	$A_{280}/A_{\lambda max}$	λ_{max}[a] (nm)	$\Delta\nu_{fwhm}$[b] (cm^{-1})	B_1[c] (nm)	B_2[d] (nm)
WT	2.5	427	4620	463	478
TM2 chimeric	4.5	425	5181	463	477
G78D	2.9	426	5150	467	480
F79L	2.7	427	4930	464	480
M81E	3.1	429	4910	464	479
C82A	8.9	422	6090		
F84L	2.6	426	4640	464	480
P88T	4.5	428	5171	464	479
V89S	3.1	425	5640	464	482
F90V	3.2	424	5460	460	482
C82A	8.9	422	6090		
F87T	9.2	412	9710		
G77R					
S85A					
S85T					
S85D	3.0	427	5090	473	474
45 K		432			
S85C					
pH 6.6	3.6	390	8333	463	462
45 K		410			
pH 8.0	2.3	365	6330		

[a] Calculated after removal (using a $1/\lambda^4$ correction factor) of light scattering from each spectrum (except VCOP and S85C) by fitting the retinal peak to a log-normal curve. [b] $\Delta\nu_{fwhm}$, full width at half-maximal absorption of the corrected retinal peak. [c] B_1, wavelength of maximal absorption of the B1 − dark difference spectrum at 45 K. [d] B_2, wavelength of maximal absorption of the B2 − dark difference spectrum at 75 K. For both B_1 and B_2, the positive band of the difference spectrum was fitted to a log-normal curve to determine the wavelength of maximal absorption.

chains were minimized on the basis of the Charmm21 force field. Following that, the binding site was minimized using PM3 semiempirical molecular orbital theory (*23*) as implemented within the MOZYME procedures of Mopac 2000.

RESULTS

Comparisons of TM2 Sequences. To identify amino acids in TM2 that could potentially play a role in structure−function in SWS1 opsins, we compared TM2 sequences across many species (Figure 1B shows selected sequences from this comparison). We found a number of highly conserved residues that were unique to the SWS1 pigments that absorb at ~425 nm, including G77, G78, F79, C82, S85, F87, P88, V89, and F90 (for comparisons, VCOP amino acid numbering is 5 less than the homologous residue in bovine rhodopsin). However, there was very little homology between groups, and we did not find any single residue between N73 at the cytoplasmic face and G96 at the extracellular face of TM2 conserved in all three classes of pigments. Both RH1 and SWS1 pigments have vicinal glycines within TM2, but they are 1−2 α-helical turns apart in the alignment. Both RH1 and M/LWS have acidic residues buried in TM2. RH1 has an abundance of hydroxyl side chains on the extracellular side of the kink, near the Schiff base linkage, while the SWS1 opsins have them more distant from the vicinal glycines. The mammalian M/LWS pigments do not have any obvious mechanism for producing a kink in TM2. Together, these observations suggest that there are significantly different interactions involving TM2 among these three classes of pigments.

TM2 Chimeric Mutant. To investigate various interactions that involve TM2 and other regions of VCOP, we replaced amino acids V72−S94 of VCOP (Figure 1B, underlined sequence), representing most of TM2, with the corresponding amino acids of bovine rhodopsin, L77−L99. This replacement left 3 out of 24 amino acids unchanged in the chimeric molecule: N73, conserved in all three families of opsins; M81, variable within SWS1; and S93, conserved in both RH1 and SWS1. Thus, this mutation effectively changes all of the amino acids embedded within the membrane bilayer, excluding the conserved helical boundaries. The chimeric mutant was expressed to the same level as VCOP in transfected COS1 cells and formed a chromophore with a λ_{max} of 425 nm when incubated with 11-*cis*-retinal, exhibiting a minor blue shift compared to wild-type VCOP (Figure 2A,D). There was a 50% reduction in the overall yield of bound retinal, reflected in the $A_{280}/A_{\lambda max}$ ratio of 4.5 versus 2.5 for wild type (Table 1). To determine whether the only unchanged residue within the membrane, M81, contributed significantly to VCOP structure, we prepared a single amino acid replacement in an otherwise wild-type VCOP background, M81E, introducing the residue found in the M/LWS opsins. The M81E protein formed a chromophore with a λ_{max} of 429 nm, exhibiting a slight red shift compared to wild type (Figure 2G). There was a 30% reduction in the overall yield of bound retinal. A comparison of the various amino acids found at position 81 shows that conservation of side chain bulk may be the important factor for this position, given its orientation into the retinal binding pocket.

We further investigated the role that TM2 plays in the formation of the primary photointermediate at cryogenic temperatures. In the dark, both TM2 chimeric and M81E mutant pigments have wild-type λ_{max} and form normal B1 at 45 K when compared to wild-type VCOP (Figure 2B,E,H). The B1 − dark difference spectra have a λ_{max} similar to that of the wild-type difference spectrum (Figure 2C,F,I, Table 1). In addition, both mutant pigments form the photostationary state B2 at 75 K as wild type, and the B2 − dark difference spectrum is similar to the wild-type difference spectrum (Figure 2B,C,E,F,H,I, Table 1).

Point Mutations. The conserved residues in TM2 were changed to probe the protonated Schiff base−chromophore interaction with this transmembrane helix. These residues were altered in VCOP by site-directed mutagenesis to the corresponding residues in either RH1 or M/LWS pigments (Figure 1B). The mutations can be classified into three categories on the basis of their spectroscopic properties: wild type, defective, or altered.

Wild-Type Mutants. In addition to the TM2 chimeric, this category includes G78D, F79L, M81E (see above), F84L, P88T, V89S, and F90V. These mutants all expressed well, exhibited retinal binding from 50% to 100% of wild type, and all formed normal photostationary states with PSS395 − dark difference spectra similar to wild type at 45 and 75 K (Table 1). There were slight shifts in the λ_{max} for some of the mutants, from 423 nm (V89S) to 428 nm (P88T) (Table 1). The apparently drastic P88T mutation (threonine in UV pigments and in most of RH1) did not result in a significant shift of λ_{max}, although retinal binding was reduced.

Defective Mutants. The C82A and F87T mutants bound retinal poorly (~10% of wild type) and exhibited blue-shifted λ_{max} compared to wild type, 422 and 412 nm, respectively (Figure 3, Table 1). The mutants were analyzed for defects in biosynthesis by Western blots. Wild-type VCOP (Figure

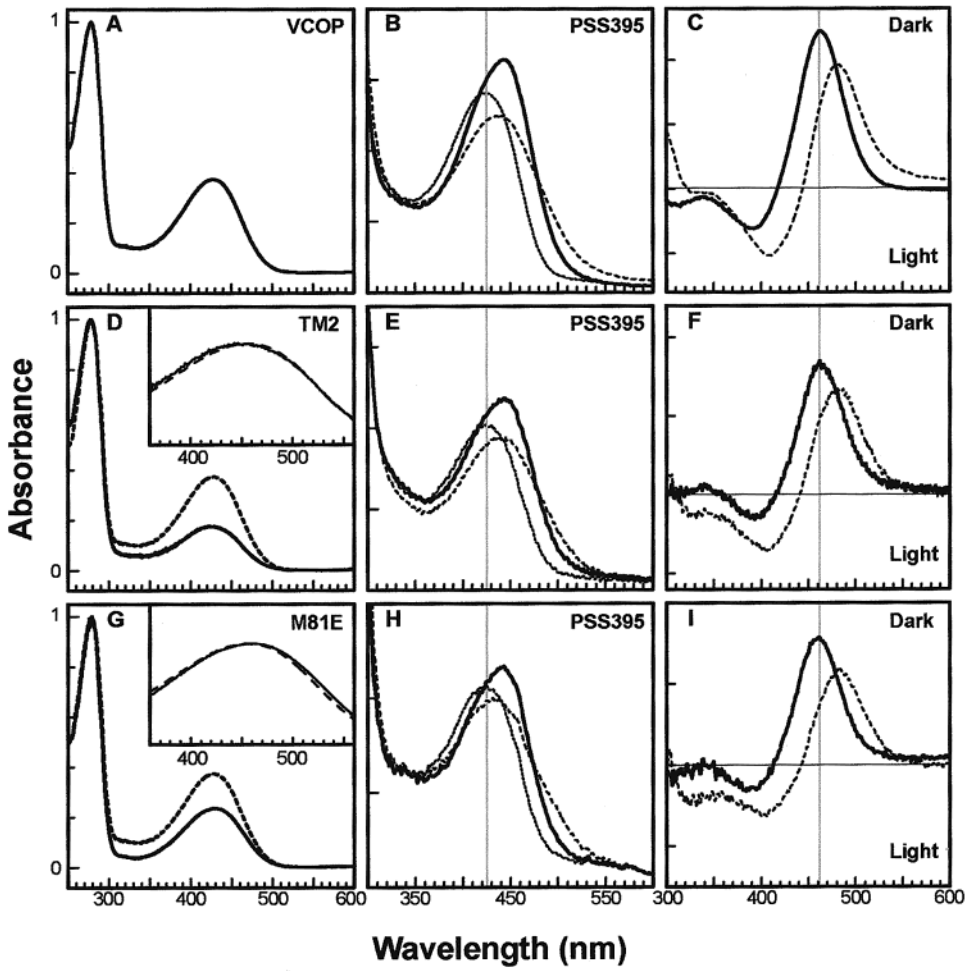

FIGURE 2: Spectroscopic profiles of VCOP, TM2 chimera, and M81E. Panels A, D, and G illustrate the absorption spectra of VCOP, TM2 chimera, and M81E at room temperature. In panels D and G, the mutant absorption spectrum (dark bold line) is overlaid with the VCOP spectrum (broken line) after normalization at A_{280}. The inset panels in D and G compare the chromophore absorbing peak of the mutant (dark line) and VCOP (broken line) after normalization at their respective λ_{max}'s. Panels B, E, and H illustrate the spectroscopic properties of VCOP, TM2 chimera, and M81E dark pigments at 45 K (thin line) and the photoproducts PSS395 at 45 K (B1, thick line) and 75 K (B2, broken line), respectively. Panels C, F, and I illustrate the B1 − dark difference spectrum at 45K (solid line) and B2 − dark difference spectrum at 75 K (broken line) of VCOP, TM2 chimera, and M81E, respectively.

4, lane 2), expressed in COS cells, migrates as an elongated smear (band I) due to heterogeneous glycosylation and a compact band (band II) with core glycosylation. Both mutants (Figure 4, lanes 4 and 7) exhibit significantly reduced levels of band I, with the amount of reduction inversely correlating with the level of bound retinal. This indicates that these mutations, while not preventing normal posttranslational modification and processing, alter the rate or folding of the apoprotein during biosynthesis (*24*, *25*). Changes in the conformation of VCOP due to the mutations may also cause the blue shift observed in the protein that stably binds retinal, suggesting that, for TM2, intrahelical interactions may be quite important for proper folding of this pigment.

G77R, S85A, and S85T do not bind retinal at all (Figure 5A,B, Table 1). The G77R mutation in the human blue cone opsin has been implicated as a cause for human tritanopia (*26*). Western analysis of G77R showed an absence of complex glycosylation and a significant amount of unglycosylated material (band III) (Figure 4, lane 3). This pattern is expected for proteins that obtain high-mannose glycosylation in the ER but do not exit the ER for further processing in the Golgi (*24*, *25*). This suggests that the G77R mutation causes misfolding of the protein and prevents complete posttranslational modifications necessary before being transported to the plasma membrane. S85A and S85T appear to have wild-type levels of glycosylated isoforms, although there is a minor amount of unglycosylated material (Figure 4, lanes 5 and 6). These mutants thus seem to be transported and inserted into the plasma membrane efficiently and fold well enough to receive the appropriate posttranslational modifications. However, the absence of retinal binding suggests that the retinal binding pocket has been significantly disturbed. Low-temperature spectroscopy could not be performed on mutants in this category.

Mutants with Altered Spectroscopic Properties. In contrast to the conservative substitutions S85A and S85T which failed to bind retinal, the mutant S85D bound retinal nearly as well as wild type and had a λ_{max} of 427 nm (Figure 5C, Table 1). To further study the effect of mutations at this position, we characterized the S85C mutant. This substitution caused a large blue shift in the λ_{max} to 390 nm (Figure 5D, Table 1). The absorbance spectrum was much broader than that of a typical visual pigment, including the mouse UV pigment (*22*), and appears to have a shoulder on the red edge of the λ_{max} band. The broadness was not due to contamination of the preparation by free retinal, because acid denaturation (*27*)

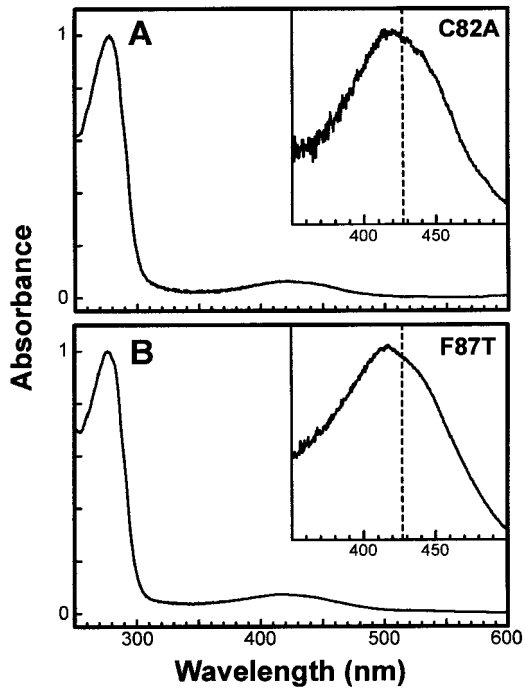

FIGURE 3: Absorption spectrum of the C82A and F87T mutants that poorly bind retinal. The inset in each panel shows a magnified view of the retinal absorbing band. The dashed line in each inset represents the λ_{max} of VCOP (λ_{max} = 427 nm).

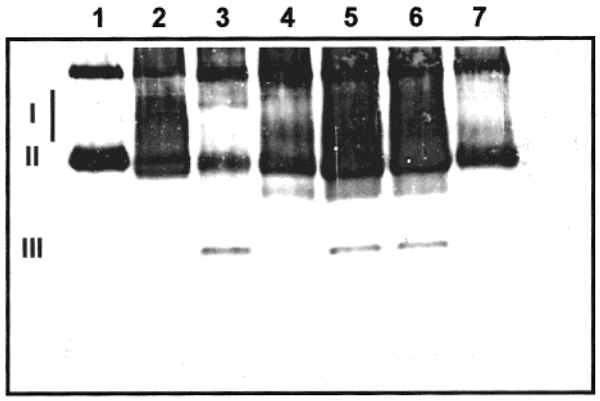

FIGURE 4: Western blot analysis of ROS (lane 1), VCOP (lane 2), G77R (lane 3), C82A (lane 4), S85A (lane 5), S85T (lane 6), and F87T (lane 7). Band I corresponds to the heterogeneously glycosylated mature form of COS cell expressed opsin. Band II corresponds to the mature form of bovine rhodopsin purified from ROS and core glycosylated monomeric opsin expressed in COS cells. Band III corresponds to unglycosylated opsin.

caused the absorbance spectrum to shift to that characteristic of a protonated retinylidene Schiff base (λ_{max} ~440 nm; data not shown). The absorption spectrum of the S85C mutant is similar to that of the pigeon SWS1 wild-type pigment (*28*). It was not possible to determine from the absorbance spectrum alone whether the retinylidene Schiff base is protonated in the S85C mutant.

We examined the effect of pH on the absorbance properties of the S85C mutant. When the pH of the protein sample was lowered from the initial 6.6, there was no significant shift in the λ_{max} until pH 4.0, at which point the λ_{max} began to shift to 440 nm (Figure 6). By pH 3.3 the λ_{max} shifts completely to 440 nm, indicating that the protein has denatured (*27*). Additional decreases in pH to 1.8 did not result in any further spectral shift (data not shown). This is

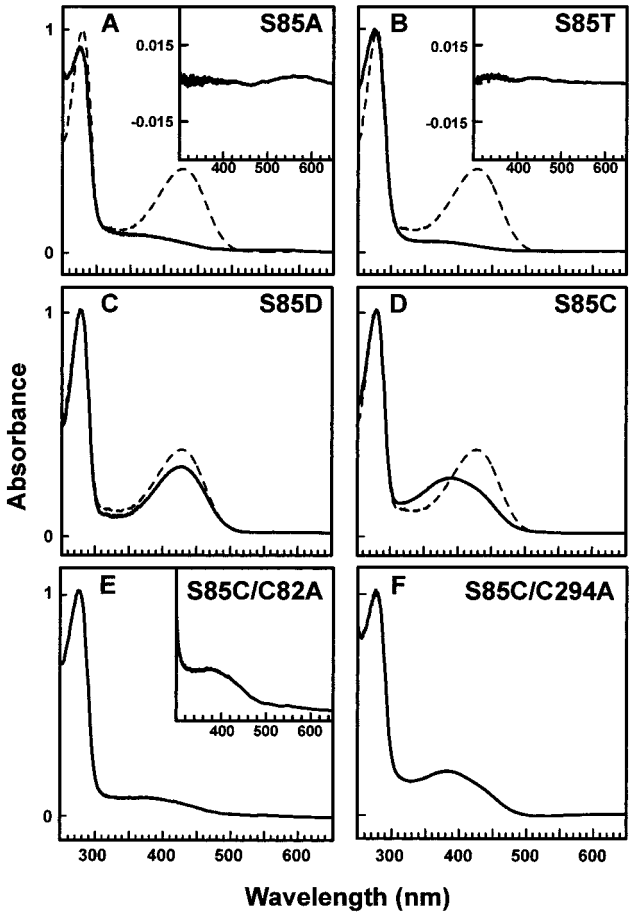

FIGURE 5: Room temperature absorption spectra of mutants at the S85 position. In the main panels, each indicated mutant spectrum (solid line) is overlaid with the VCOP spectrum (broken line). A light − dark difference spectra are shown in the insets for the S85A and S85T mutants. The inset in panel E shows a magnified view of the S85C/C82A chromophore band.

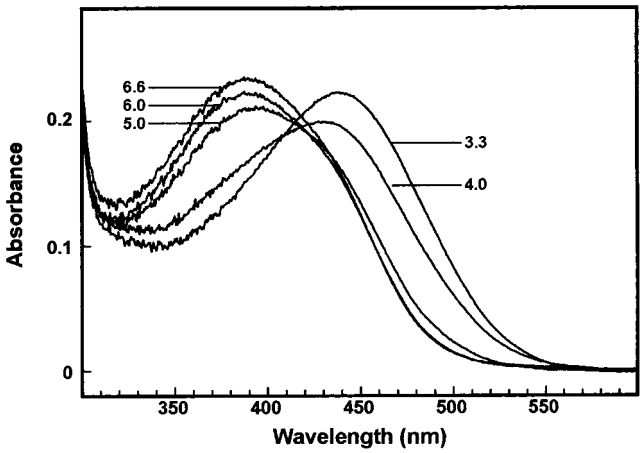

FIGURE 6: Absorption spectrum profile of the S85C mutant at acidic pHs. The initial pH was 6.6 and was subsequently lowered to the indicated pHs.

quite similar to wild-type VCOP, which denatures at pH 3.3 (data not shown). The behavior of the S85C pigment was also investigated at pH >6.6. From pH 6.6 to pH 7.1, the absorption profile did not show any change (data not shown). However, at pH 7.5 and above, the λ_{max} shifted to 365 nm and the absorbance spectrum narrowed to a full width at half-maximum similar to that of the mouse UV pigment (*22*)

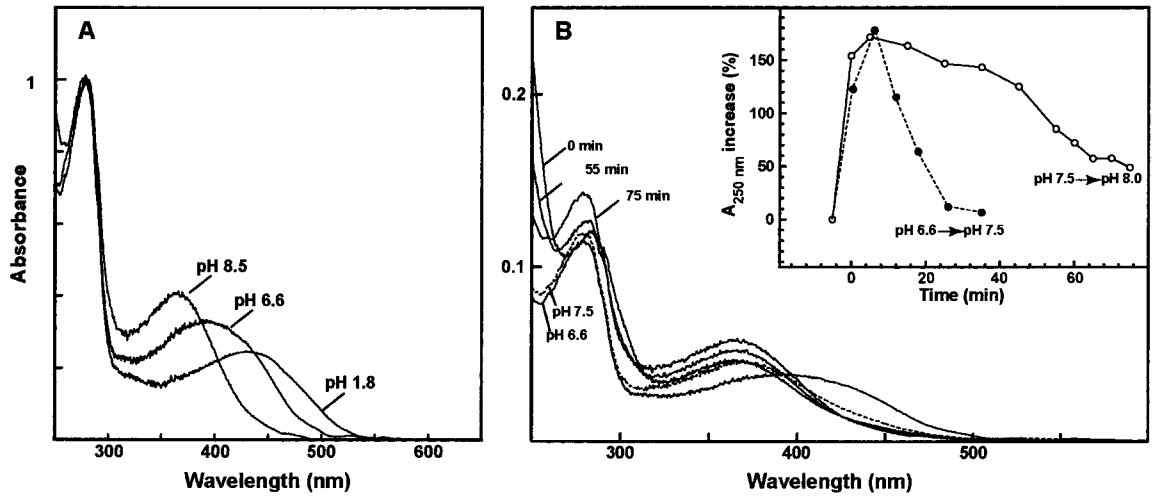

FIGURE 7: Absorption spectrum profile of the S85C mutant at basic pHs. Panel A illustrates the spectral profile of the mutant at the indicated pHs. Samples were titrated from a pH of 6.6−8.5. The pH was subsequently dropped to 1.8. Panel B illustrates the distortion of the protein peak at pH 7.5 and 8.0 at various time intervals after incubation at the indicated pH. The inset panel is a graphic summary of the change in A_{250} as a function of time at the indicated pH transitions.

(Table 1 and Figure 7A). The absorbance spectrum is consistent with an unprotonated retinylidene Schiff base linkage (*29*), and this observation raises the possibility that the species with λ_{max} 390 nm is protonated, and increasing the pH leads to a deprotonation of the Schiff base. Upon subsequent lowering of the pH from 7.5 and above, there was no change in the absorption spectrum until pH 4.0, at which point the protein begins to acid denature (data not shown).

When the pH was raised above 7.5, there was a transient increase in the absorbance of the samples in the UV region resulting in a dramatic distortion of the protein absorbance peak (A_{280}). The protein absorbance rapidly increased after the pH change (1−2 min) and then slowly recovered to the starting value. The time to recover depended upon the pH and took more than 1 h at pH >8.0 (Figure 7B). Control experiments indicated that the increase in absorbance was not due to changes in the buffer or hydrolysis of the retinylidene Schiff base, since acid denaturation of the pH 8.5 pigment showed that the retinal was still covalently attached to the protein (Figure 7A). The increase in UV absorbance may reflect a reversible aggregation of the S85C mutant or a change in the micellar structure that leads to a transient increase in light scattering. These results suggest that there is a protein conformational change that occurs upon raising the pH, which may accompany deprotonation of the Schiff base or other rearrangements of the retinal binding pocket.

An examination of a model of VCOP (*19*) based upon the rhodopsin crystal structure suggests that the S85C mutation could potentially form an intramembrane disulfide bond with one of two membrane-embedded Cys residues: C82 and C294. To determine whether the absorbance properties reflected the formation of such a bond, double mutants were prepared to eliminate the potential for these disulfide linkages: S85C/C82A and S85C/C294A. Both mutants bound retinal and formed a chromophore with absorbance spectra that had the same λ_{max} and broad shape as the single mutant S85C (Figure 5E,F). The efficiency of retinal binding was lower in the case of the S85C/C82A double mutant, reflecting the reduced formation of chromophore in the single C82A mutant. Thus, the S85C mutation was dominant and did not involve a disulfide bond formation with either residue. These results suggest that the S85C mutation is exerting its effect by changing the retinylidene Schiff base environment.

The S85D mutant exhibits a red-shifted λ_{max} of 432 nm when cooled to 45 K in the dark (Figure 8D, Figure 9), and illumination produces a B1 state (Figure 8E). The B1 − dark difference spectrum was red shifted by ∼10 nm compared to the wild-type difference spectrum (Figure 8F, Table 1). The calculated batho intermediate (Figure 9) is also red shifted by ∼20 nm (λ_{max} ∼470 nm) compared to the wild-type batho intermediate (λ_{max} ∼450 nm). Illumination of the dark state at 75 K produced a B2 state and the B2 − dark difference spectrum has a similar λ_{max} compared to the B1 − dark difference spectrum (Figure 8F, Table 1). There was no change in the absorption spectrum of B2 upon warming until 200 K, when the lumi intermediate begins to form (data not shown).

The S85C (pH6.6) mutant exhibits a large 20 nm red shift to λ_{max} ∼410 nm upon cooling in the dark (Figures 8A and 9). This shift was accompanied by a decrease in the full width at half-maximum to a wild-type value. Illumination produces a B1 state and the B1 − dark spectrum has a λ_{max} of ∼463 nm (Figure 8B,C and Table 1). The calculated batho intermediate formed at 45 K has a λ_{max} of ∼465 nm, red shifted compared to the wild-type batho intermediate by 15 nm (Figure 9). Illumination of the dark state at 75 K produces a B2 state, and the B2 − dark difference spectrum has a λ_{max} of ∼462 nm (Figure 8B,C and Table 1).

Thus, both S85D and S85C substitutions cause a change in the retinylidene Schiff base environment of the primary photointermediate, reflected in a red-shifted batho intermediate (Figure 9) compared to the wild-type batho intermediate. While the nature of the molecular interactions remains unresolved for now, it is clear that the individual batho species are different in both an absolute and a relative sense from the batho state observed in the native VCOP protein. The red shift in forming batho in VCOP is about 1200 cm^{-1}, smaller than the corresponding shift in S85D (∼1900 cm^{-1}), and both values are much smaller than in S85C (∼2900

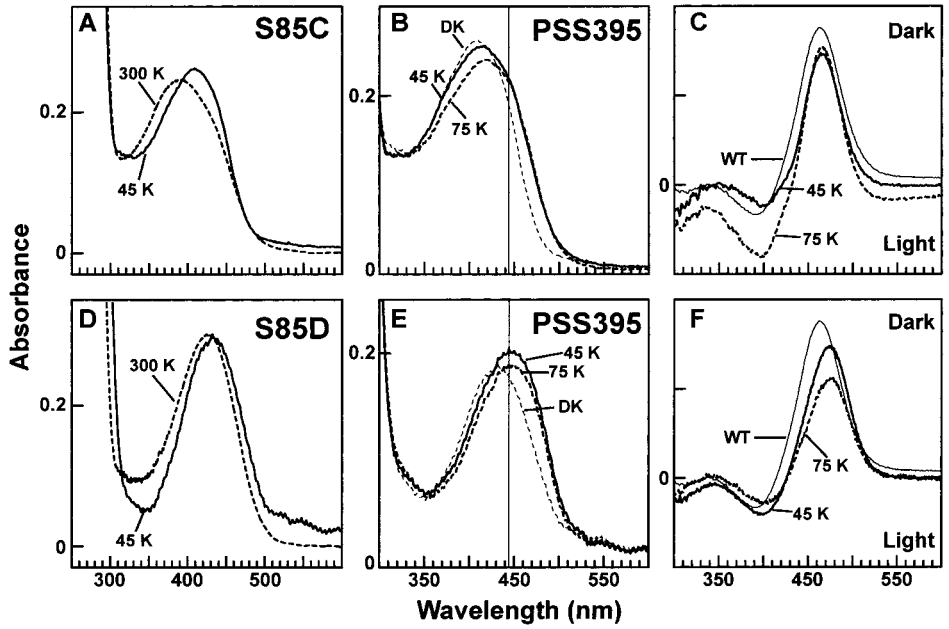

FIGURE 8: Absorption spectra of the S85C and S85D mutants and their photoproducts at cryogenic temperatures. Panels A and D indicate the spectrum of dark samples at room temperature (broken line) and at 45 K (solid line). Panels B and E illustrate the dark spectrum at 45 K (thin broken line), PSS395 (B1) at 45 K (solid line), and PSS395 at 75 K (B2) (thick dashed line) of the S85C and S85D mutants. The horizontal line represents the λ_{max} for the wild-type PSS395 (B1) state at 45 K. Panels C and F illustrate the B1 − dark difference spectrum (bold solid line) and B2 − dark difference spectrum (broken line) of the S85C and S85D mutants, respectively. In panels C and F, the wild-type B1 − dark difference spectrum is displayed (thin solid line).

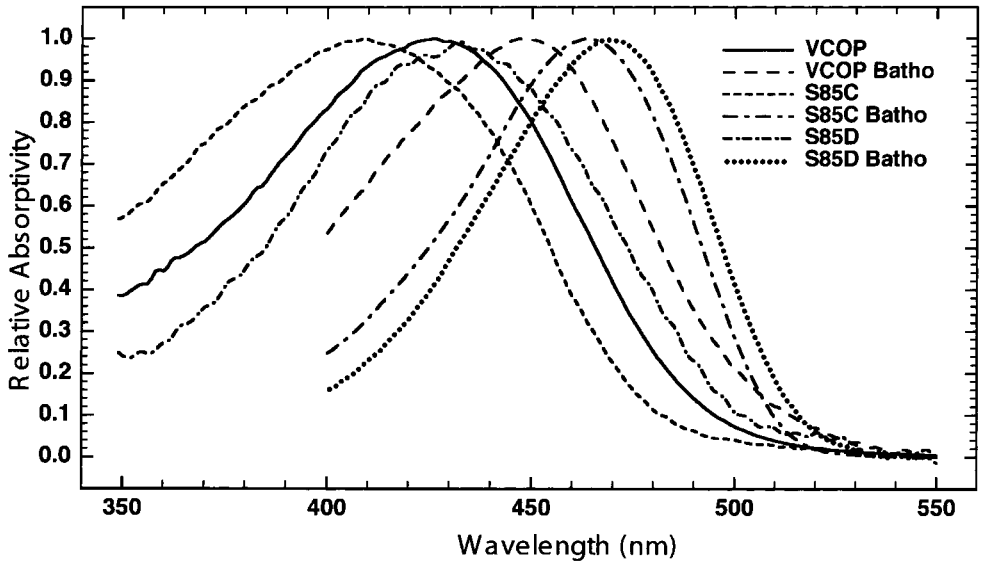

FIGURE 9: Dark and the calculated batho intermediate for VCOP, S85D, and S85C at 45 K.

cm^{-1}). These values provide insight into the importance of S85 in mediating the electrostatic environment in both the resting state and the primary photoproduct. Given the constraints upon protein movements possible at such low temperature, these results suggest that the S85 mutants may interact directly with the counterion to change the chromophore properties and presumably indicate that S85 is very close to the counterion in the wild-type pigment.

DISCUSSION

We have identified a number of amino acids in TM2 of VCOP that are essential for retinal binding, including C82, S85, and F87. We have found a significant role for S85 in maintaining the steric and electrostatic properties of the SWS1 binding pocket. We characterized six mutants at this position, whose phenotypes at room temperature ranged from wild type, blue shifted, or unable to bind retinal. We hypothesize that the amino acid side chain at the S85 position directly interacts with the Schiff base counterion. We also examined the spectral properties of a mutant in which TM2 in VCOP was replaced with a homologous sequence from bovine rhodopsin. Surprisingly, in light of the lack of any significant conservation between VCOP and bovine rhodopsin TM2, including a glycine at the S85 position, the mutant exhibited wild-type properties. In the following section, we describe the rationale for our hypothesis that the S85 side chain is interacting directly with the protonated Schiff base counterion, and then we discuss how

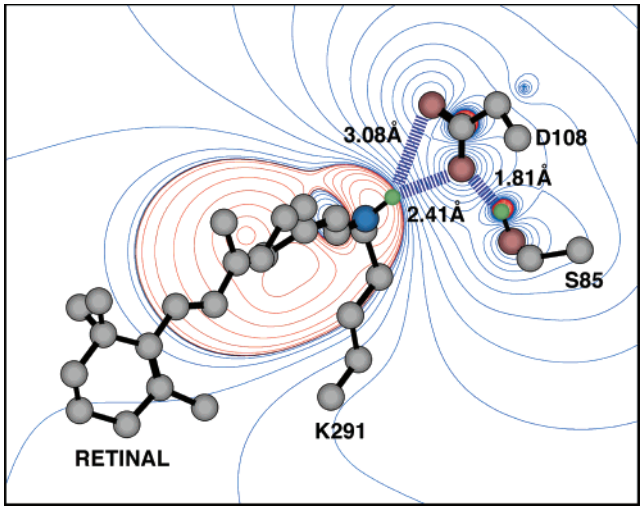

FIGURE 10: Binding site model of VCOP showing the relative position of the 11-*cis*-retinal chromophore, the counterion D108, and S85. Key distances and electrostatic interactions are shown using dashed lines. The electrostatic energy associated with the interaction of a bare positive charge (+e) moving in the plane defined by the imine proton, D108 carboxylate carbon, and S85 hydroxyl oxygen is shown using field contours. Blue contours indicate negative energy (attraction) and red indicate positive energy (repulsion) between the positive charge and the atomic charges based on PM3 MO theory. The contour levels in J/mol are as follows: 0, ±4, ±30, ±100, ±240, ±460, ±800, ±1300, ±1900, ±2700, ±3700, ±4900, ±6400, ±8100, ±10000, ±12000, ±15000, ±18000, ±22000, ±25000, and ±30000.

this model can explain the observed behavior of the VCOP TM2 mutants, including the TM2 chimeric.

Interaction of S85 with the Retinylidene Counterion: Theoretical Considerations. The crystal structure of rhodopsin (*15*) was used as a template to produce a model of VCOP, in which the side chain orientations were assigned using position-specific rotamer libraries and refined using multiple molecular dynamics (MD) simulations to access local conformations (*19*). The resulting structure placed S85 close enough to the Schiff base counterion to participate in a hydrogen bond with a carboxylate oxygen atom of the Schiff base counterion, D108 (Figure 10). The counterion is held in a conformation that allows close interaction with the protonated retinylidine imine Schiff base linkage, but D108 is in a rather tenuous location. It is too close to the Schiff base to permit mediation via a bridging water molecule but too far away to form a strong hydrogen bond. The model suggests that the role of S85 is to facilitate the electrostatic stabilization of the protonated Schiff base by forming a very strong hydrogen bond to the D108 counterion. This interaction would tend to decrease the extent to which the chromophore is blue shifted by the primary counterion (D108). From the above comments, alteration of the S85 hydrogen bond would be expected to blue shift the absorption spectrum and destabilize the protonated Schiff base. A more quantitative picture can be obtained by calculating the relative energy of the ground state interaction with D108 for substitution at position 85: alanine (S85A, +11.7 kcal/mol), serine (native, 0 by definition), cysteine (S85C, −2.16 kcal/mol), aspartate (S85D, neutral, −11.5 kcal/mol). These numbers are based on PM3 semiempirical molecular orbital theory and are very approximate because only a partial minimization of the surrounding protein was carried out. Nevertheless, it is clear that removal of the hydrogen bond (S85A) has a significant destabilization of the ground state, while introduction of another hydrogen-bonding residue with more conformational flexibility (S85D) stabilizes the protonated Schiff base. In the case of S85C, the calculations suggest that little if any change would be observed, and yet we get a large blue shift. This points out another facet of the interaction of S85 with D108, that steric effects may play an important role in the retinylidene Schiff base environment, and suggests that the anomalous blue shift observed in S85C is due, at least in part, to such steric effects.

Interaction of S85 with the Retinylidene Counterion: S85 Mutants. In the wild-type pigment, S85 is clearly buried within the lipid bilayer, and thus the hydrophobic environment will make it energetically favorable for the polar S85 side chain to be involved in the formation of a hydrogen bond, either with the peptide backbone of TM2 (*30*) or with the carboxylate group of the counterion to the protonated Schiff base. The mutagenesis data, as well as the model described above, support the latter possibility.

The mutant S85D has wild-type spectral properties at room temperature. The lack of any spectral shift strongly argues that the introduced carboxylate is uncharged (protonated). Although it is conceivable that S85D could become the primary counterion, replacing D108, it does not seem likely that this could occur without a change in the λ_{max}. The low-temperature results indicate that S85D is in the vicinity of the Schiff base since it causes a red shift of the primary photointermediate as well as the dark state, and thus the protonated carboxylate of S85D is available to interact with the counterion. At low temperature, the S85C mutant shows a large red shift and forms a batho state that is further red shifted. These results support the idea that the Schiff base in S85C is protonated at pH 6.6, like the wild-type pigment. The weaker hydrogen-bonding characteristics of Cys compared to Ser could account, in part, for the large blue shift observed in the mutant, by destabilizing the position of the counterion. Moreover, to accommodate the bulky sulfhydryl group, the position of the counterion relative to the Schiff base could also be disturbed, leading to spectral shifts. Although it is possible that mutations at S85 induce changes in the retinal chromophore itself, this does not seem likely on the basis of the rhodopsin structure, in which TM2 is not in close contact with retinal (*15*).

If, as we have supposed, the S85C pigment has a protonated Schiff base at pH 6.6, then as the pH is increased above 7, the Schiff base certainly becomes deprotonated. This can be concluded since the λ_{max} shifts to 365 nm [identical to an unprotonated retinylidene Schiff base (*29*)] and the shape of the absorption spectrum changes to that found for other UV opsins, such as mouse UV (*22*, *28*). The deprotonation of the Schiff base as the pH is raised occurs with a significant conformational rearrangement of the protein that can be detected by transient changes in UV absorption. One possible mechanism for this change might involve a two-step process, in which the sulfhydryl group would first deprotonate and lose the interaction with the counterion, perhaps even destabilizing the counterion−Schiff base interaction. In the second step, the Schiff base could subsequently deprotonate. Alternatively, increasing the pH of the S85C pigment could cause changes in conformation that could result more indirectly in alterations of the interactions of the S85C−D108−Schiff base moieties.

The inability of the S85A and S85T mutants to bind retinal also supports the idea that S85 interacts with the counterion. The neutral side chain of alanine would be unable to form a hydrogen bond with the counterion and consequently be oriented with the bulky side chain methyl group away from the polar counterion and into the binding pocket. The S85T might be expected to form a hydrogen bond with the counterion, but at the same time the bulky Cγ methyl group would be oriented toward the binding pocket. Thus these two mutations potentially interfere with retinal binding due to the introduction of extra methyl groups into the binding pocket.

We cannot rule out the possibility that S85 is forming a pH-dependent hydrogen bond with another residue which is indirectly responsible for maintaining protein structure and function. We note, however, that our dynamics simulations uncovered no interactions of S85 with other residues (or the protein backbone) of any energetic or temporal consequence.

The S85 position in other SWS1 pigments has been studied by several groups (*12*−*14*, *31*). In human SWS1, S85G folded poorly with an approximate λ_{max} of 404 nm (*12*). In the budgerigar SWS1 which absorbs in the UV, mutation of a Cys at this position to a Ser results in a 35 nm red shift from 363 to 398 nm (*31*). In the zebra finch UV pigment, the same mutation caused a 40 nm red shift (*13*). Moreover, significant blue shifts occurred when Ser was changed to Cys in other avian SWS1 pigments with λ_{max} ∼420 nm (*13*). All of the Cys-containing mutant pigments exhibited a broad retinal absorption band in the UV region at pH 6.6. However, in contrast to our results, the absorbance properties of the avian Cys 85 containing SWS1 pigments did not change at pH >7. One possible reason for this could be different buffer compositions of the various studies. What is clear from these studies is the important role for the S85 position in spectral tuning, which we hypothesize involves interactions with the Schiff base counterion.

Interaction of S85 with the Retinylidene Counterion: TM2 Chimeric. According to sequence alignments, this helix replacement mutant places a glycine at the position occupied by serine in the center of the TM2. However, our mutagenesis data indicate that such a mutation should have caused the pigment to deviate from the wild-type characteristics. The crystal structure of bovine rhodopsin (*15*) places the residue T94 ∼3.4 Å away from one of the oxygens of the counterion and, thus, is in a potential hydrogen bond. Moreover, T94 is one helical turn from the kink orienting G90 toward the extracellular face. To account for the TM2 chimeric data, we suggest that the bovine rhodopsin TM2 is sufficiently flexible to bring about an interaction between T94 and the counterion in the chimeric pigment. Such a flexibility seems likely due to the presence of glycines (89 and 90) in the center of the bovine rhodopsin TM2 helix.

TM2−*Counterion Interactions in Other Visual Pigments.* Acidic and polar mutations at position G90 in bovine rhodopsin lead to significant λ_{max} shifts of the dark state (*11*, *16*). From this it is expected that changing the corresponding S85 residue to neutral, acidic residues should lead to correlated λ_{max} shifts in SWS1 pigments. As clearly evident from our study and others, this is not the case. A comparison of the SWS1 and RH1 TM2 sequences indicates that the kink-inducing vicinal glycines are approximately 1−2 helical turns apart in the alignment. Thus in the case of rhodopsins, the kink causes the G90 to come in proximity to the counterion. Any acidic or polar mutation at this position will allow a direct interaction between this residue and the Schiff base−chromophore. On the other hand, the kink in TM2 of SWS1 pigments presumably occurs 1−2 helical turns further up the helix toward the cytoplasmic face. This would place the S85 residue at a much more distal position with respect to the Schiff base−chromophore region compared to S90 in bovine rhodopsin. Consequently, in SWS1 pigments, the S85 position would favor a stronger hydrogen bond with the counterion than with the more distant chromophore−Schiff base. Owing to the differences in these contacts, mutagenesis data at this position from SWS1 and the G90 position in bovine rhodopsin would have little relationship to each other.

In SWS1 pigments, S85 is located approximately 1−2 helical turns from the helical kink toward the extracellular face. Similarly, the crystal structure of bovine rhodopsin places T94 approximately one helical turn from the kink toward the extracellular face and in close contact with the counterion (*15*). From this, it appears that, in SWS1 and RH1 pigments, the location of the glycine-induced kink in TM2 and the polar residue from TM2 that interacts with the counterion are related in terms of their location with respect to each other. Thus, it is tempting to speculate that the location and the functional purpose of the kink in TM2 are to appropriately orient the polar residue in TM2 for optimal interaction and stabilization of the counterion to the protonated Schiff base. It is not clear whether these ideas apply to the M/LWS pigments and other visual pigments that lack any potential kinks or obvious flexibility in TM2.

The mouse SWS1 pigment has a λ_{max} of ∼360 nm presumably due to a deprotonated Schiff base (*22*, *28*), although it contains the vicinal glycines and S85 in TM2. One way of achieving a deprotonation of the Schiff base would be to destabilize the interaction between the counterion and the protonated Schiff base. This could be achieved by altering the position of the counterion relative to S85 so that the S85 no longer interacts with the counterion. Again, this would mean that the S85 side chain would be oriented toward the binding pocket and possibly interfere with retinal binding. To accommodate the change in the orientation of the serine, we would predict that further mutations that alter the relative orientation of the chromophore in the binding pocket would be needed to permit retinal binding, such as mutations near the C9 methyl group of retinal. The recent work on mammalian SWS1 pigments supports this mechanism for achieving deprotonation of the Schiff base (*14*).

In summary, both theoretical considerations and mutagenesis data support our hypothesis that the S85 side chain in SWS1 pigments interacts directly with the protonated Schiff base counterion. This has led us to propose that this interaction plays a crucial role in spectral tuning in SWS1 pigments. This model, a combination of the counterion−Schiff base interaction and the S85−counterion interaction, which we term the *extended counterion*, supposes a key role for both the counterion and its hydrogen-bonding partner in determining the spectral properties of the short-wavelength visual pigments and the microenvironment of the Schiff base encompassed by TM2, TM3, and TM7. Extended counterion interactions may also play an important role in determining the functional properties of other classes of vertebrate and invertebrate visual pigments.

REFERENCES

1. Ebrey, T., and Koutalos, Y. (2001) *Prog. Retinal Eye Res. 20*, 49−94.
2. Wald, G. (1968) *Nature 219*, 800−808.
3. Khorana, H. G. (1986) *Ann. N.Y. Acad. Sci. (Int. Symp. Bioorg. Chem.) 471*, 272−288.
4. Yoshizawa, T., and Shichida, Y. (1982) in *Methods in Enzymology*, pp 333−354, Academic Press, Inc., New York.
5. Kliger, D. S., and Lewis, J. W. (1995) *Isr. J. Chem. 35*, 289−307.
6. Stryer, L. (1986) *Annu. Rev. Neurosci. 9*, 87−119.
7. Rodieck, R. W. (1998) *The First Steps in Seeing*, Sinauer Associates, Inc., Sunderland, MA.
8. Schnapf, J., and Baylor, D. A. (1986) *Sci. Am. 256*, 32−39.
9. Imai, H., Imamoto, Y., Yoshizawa, T., and Shichida, Y. (1995) *Biochemistry 34*, 10525−10531.
10. Imai, H., Kojima, D., Oura, T., Tachibanaki, S., and Terakita, A. (1997) *Proc. Natl. Acad. Sci. U.S.A. 94*, 2322−2326.
11. Lin, S. W., Kochendoerfer, G. G., Carroll, K. S., Wang, D., Mathies, R. A., and Sakmar, T. P. (1998) *J. Biol. Chem. 273*, 24583−24591.
12. Fasick, J., Lee, N., and Oprian, D. (1999) *Biochemistry 38*, 11593−11596.
13. Yokoyama, S., Radlwimmer, F., and Blow, N. (2000) *Proc. Natl. Acad. Sci. U.S.A. 97*, 7366−7371.
14. Yokoyama, S., and Shi, Y. (2000) *FEBS Lett. 486*, 167−172.
15. Palczewski, K., Kumasaka, T., Hori, T., Behnke, C. A., Motoshima, H., Fox, B. A., Le Trong, I., Teller, D. C., Okada, T., Stenkamp, R. E., Yamamoto, M., and Miyano, M. (2000) *Science 289*, 739−745.
16. Rao, V. R., Cohen, G. B., and Oprian, D. D. (1994) *Nature 367*, 639−642.
17. Zvyaga, T., Fahmy, K., Siebert, F., and Sakmar, T. (1996) *Biochemistry 35*, 7536−7545.
18. Starace, D. M., and Knox, B. E. (1998) *Exp. Eye Res. 67*, 209−220.
19. Kusnetzow, A., Dukkipati, A., Babu, K. R., Singh, D., Vought, B. W., Knox, B. E., and Birge, R. R. (2001) *Biochemistry 40*, 7832−7844.
20. Starace, D. M., and Knox, B. E. (1997) *J. Biol. Chem. 272*, 1095−1100.
21. Molday, R. S., and MacKenzie, D. (1983) *Biochemistry 22*, 653−660.
22. Vought, B. W., Dukkipatti, A., Max, M., Knox, B. E., and Birge, R. R. (1999) *Biochemistry 38*, 11287−11297.
23. Stewart, J. J. P. (1989) *J. Comput. Chem. 10*, 221−245.
24. Nakayama, T. A., Zhang, W., Cowan, A., and Kung, M. (1998) *Biochemistry 37*, 17487−17494.
25. Kaushal, S., and Khorana, H. G. (1994) *Biochemistry 33*, 6121−6128.
26. Weitz, C. J., Miyake, Y., Shinzato, K., Montag, E., Zrenner, E., Went, L. N., and Nathans, J. (1992) *Am. J. Hum. Genet. 50*, 498−507.
27. Kito, Y., Suzuki, T., Azuma, M., and Sekoguti, Y. (1968) *Nature 218*, 955−957.
28. Yokoyama, S., Radlwimmer, F. B., and Kawamura, S. (1998) *FEBS Lett. 423*, 155−158.
29. Blatz, P. E., Mohler, J. H., and Navangul, H. V. (1972) *Biochemistry 11*, 848−855.
30. Gray, T. M., and Matthews, B. W. (1984) *J. Mol. Biol. 175*, 75−81.
31. Wilkie, S. E., Robinson, P. R., Cronin, T. W., Poopalasundaram, S., Bowmaker, J. K., and Hunt, D. M. (2000) *Biochemistry 39*, 7895−7901.

BI011354L